



**Ferric reducing reactivity assay with theoretical kinetic modeling uncovers electron transfer schemes of metallic-nanoparticle-mediated redox in water solutions**

Journal:	<i>Environmental Science: Nano</i>
Manuscript ID	EN-ART-03-2019-000258.R1
Article Type:	Paper
Date Submitted by the Author:	30-Apr-2019
Complete List of Authors:	Bi, Xiangyu; Connecticut Agricultural Experiment Station, Environmental Sciences Westerhoff, Paul; Arizona State University, Dept. of Civil and Environ. Engineering

1  
2  
3 **Ferric reducing reactivity assay with theoretical kinetic modeling uncovers electron**  
4 **transfer schemes of metallic-nanoparticle-mediated redox in water solutions**  
5  
6

7 Xiangyu Bi\* and Paul Westerhoff  
8  
9

10  
11  
12 School of Sustainable Engineering and the Built Environment, Arizona State University,  
13  
14 Tempe, Arizona, USA  
15

16  
17 \*Correspondence: E: [xiangyu.bi@asu.edu](mailto:xiangyu.bi@asu.edu)  
18

19 **In preparation for submission to *Environmental Science: Nano***  
20  
21

22  
23  
24 **ENVIRONMENTAL SIGNIFICANCE**  
25

26 Redox processes mediated by metallic nanoparticles (NPs) in water solutions are  
27  
28 highly relevant to the NPs' toxicity to biological systems via generating reactive oxygen  
29  
30 species and causing oxidative stress. Probing NP surface reactivity of mediating  
31  
32 interfacial electron transfer is thus important to nanomaterial risk assessment. Current  
33  
34 chemical assays, despite their ability to report relative reactivity magnitudes of different  
35  
36 NP species, hardly manifest assay reaction mechanisms, which, however, is critical to  
37  
38 interpreting reactivity measurement results accurately and avoiding misleading  
39  
40 comparisons of reactivity magnitudes over different reaction mechanisms. We  
41  
42 demonstrate theoretical modeling of reaction kinetics enables a chemical assay to not  
43  
44 only measure NP reactivity magnitude, but also uncover interfacial electron transfer  
45  
46 schemes underlying the assay reaction mechanism.  
47  
48  
49  
50  
51  
52  
53  
54  
55  
56  
57  
58  
59  
60

1  
2  
3 **Ferric reducing reactivity assay with theoretical kinetic modeling uncovers electron**  
4 **transfer schemes of metallic-nanoparticle-mediated redox in water solutions**  
5  
6

7  
8 Xiangyu Bi\* and Paul Westerhoff  
9

10  
11  
12 School of Sustainable Engineering and the Built Environment, Arizona State University,  
13  
14 Tempe, Arizona, USA  
15

16  
17 \*Correspondence: E: [xiangyu.bi@asu.edu](mailto:xiangyu.bi@asu.edu)  
18

19 **In preparation for submission to *Environmental Science: Nano***  
20  
21  
22  
23  
24  
25  
26  
27  
28  
29  
30  
31  
32  
33  
34  
35  
36  
37  
38  
39  
40  
41  
42  
43  
44  
45  
46  
47  
48  
49  
50  
51  
52  
53  
54  
55  
56  
57  
58  
59  
60

**ABSTRACT**

1  
2  
3  
4  
5  
6  
7  
8  
9  
10  
11  
12  
13  
14  
15  
16  
17  
18  
19  
20  
21  
22  
23  
24  
25  
26  
27  
28  
29  
30  
31  
32  
33  
34  
35  
36  
37  
38  
39  
40  
41  
42  
43  
44  
45  
46  
47  
48  
49  
50  
51  
52  
53  
54  
55  
56  
57  
58  
59  
60

Metallic nanoparticles (NPs) can mediate electron transfer in water solutions. We report a chemical assay named “ferric reducing ability of nanoparticles” (FRAN), which is capable of probing electron fluxes at NP-water interfaces. The assay provides time-resolved colorimetric analysis for evaluating the surface reactivity of metallic NPs in redox processes and in elucidating the electron transfer schemes. FRAN includes the reduction of ferric ( $\text{Fe}^{\text{III}}$ ) to ferrous ( $\text{Fe}^{\text{II}}$ ) ions by electrons transferred from NPs at the NP-water interface. In tests of 20-nm gold (Au) and silver (Ag) NPs, the plateaued  $\text{Fe}^{\text{II}}$  concentration after reaction time was linearly correlated to the NP concentration. However, distinct kinetic trends, which are mathematically described by an exponential and logarithmic function, were observed between Ag and Au NPs. We developed two theoretical models, which infer two interfacial electron transfer schemes, to explain the difference between materials. For Ag NPs, the occurring redox is a one-electron transfer from  $\text{Ag}^0$  to  $\text{Fe}^{\text{III}}$ , leading to formation of  $\text{Ag}^+$  and  $\text{Fe}^{\text{II}}$ . Being a heterogeneous reaction including the NP solid and aqueous solution, it involves electron transfer at the interfacial region in which the collision between  $\text{Fe}^{\text{III}}$  and  $\text{Ag}^0$  acts homogeneously, and thus its kinetics behaves as a pseudo first-order reaction. For Au NPs, an electron flux forms when electrons stored in the NP phase are “discharged” like an electrode to reduce  $\text{Fe}^{3+}$  at the interface, and the NPs act as electrodes. The experiments and models for FRAN can aid in design of NP antioxidant functionality and assessment of environmental impacts of NPs in water or other fluids.

## INTRODUCTION

1  
2  
3  
4  
5  
6  
7  
8  
9  
10  
11  
12  
13  
14  
15  
16  
17  
18  
19  
20  
21  
22  
23  
24  
25  
26  
27  
28  
29  
30

Metallic nanoparticles (NPs) in aqueous solutions can mediate electron transfer at interfaces due to their surface reactivity. Surface reactivity of metallic NPs has led not only to their applications in heterogeneous catalysis,<sup>1</sup> nano-medicine,<sup>2</sup> antibacterial agent,<sup>3,4</sup> and nano-coatings,<sup>5,6</sup> but also to recognition of potential hazards to environmental and human health via interrupting regular redox processes,<sup>7</sup> damaging cell membranes,<sup>8,9</sup> or generating unpleasant redox active matters such as the reactive oxygen species (ROS).<sup>10,11</sup> While analytical methods are emerging to quantify elemental mass and composition of NPs in aqueous matrices,<sup>12-14</sup> methods of assessing NP surface reactivity in regard to mediating electron transfer could be more informative to NP risk assessment or transformation in surface reactive after entering complex environmental matrices (*i.e.*, NP aging).

31  
32  
33  
34  
35  
36  
37  
38  
39  
40  
41  
42  
43  
44  
45  
46  
47  
48  
49  
50  
51  
52  
53  
54  
55  
56  
57  
58  
59  
60

Surface reactivity of NPs in aqueous matrices is commonly assessed by initiating reactions at NP-solution interfaces. Various probe molecules (*e.g.*, p-nitrophenol,<sup>15</sup> ferrocyanate,<sup>16</sup> and methylene blue (MB)<sup>17</sup>) have been used to directly implement these reactions by acting as electron donor or acceptor at the interface, while others rely on different spectrometry<sup>18</sup> to detect occurring interfacial reactions that are relevant to NPs' risks associated with a ROS formation. These assays are based on well-controlled reaction conditions and measure a parameter (*e.g.*, a reaction rate constant or reactant/product concentration in a steady state) to indicate the surface reactivity magnitude or ROS formation potentials. In many cases, the operating method of a reactivity assay was developed for dissolved chemicals and then extended to NPs. However, such assays designed for homogeneous reactions may have different operating mechanisms when applied to heterogeneous matrices such as NPs in water. Specifically,

1  
2  
3 the role of interfacial reaction mechanisms on the assays remains poorly documented.  
4  
5 This issue is critical because without a fundamental understanding of how different NP  
6  
7 surfaces may mediate electron transfers differently, the outcome variance among  
8  
9 different assays<sup>19, 20</sup> cannot be well understood, leading to confusing or biased analysis.  
10  
11 Meanwhile, correlations between different reactivity and toxicity assays have been  
12  
13 reported,<sup>11, 19, 21</sup> but there is a lack of knowledge demonstrating which reactivity assay(s)  
14  
15 would accurately predict a NP species' hazard.  
16  
17

18  
19 We herein seek an assay that can, in addition to evaluate surface reactivity magnitude,  
20  
21 provide quantitative insights into the electron transfer scheme at the NP and water  
22  
23 solution interfaces. Benzie and Strain introduced the “ferric reducing ability of plasma  
24  
25 (FRAP) assay,<sup>22</sup> which uses the degree to which the ferric (Fe<sup>III</sup>) ions get reduced by any  
26  
27 reducing agents in a plasma medium to suggest a total “antioxidant power” of the plasma.  
28  
29 FRAP is easy to operate and has been widely used to assess the antioxidant power of  
30  
31 dilatory product,<sup>23</sup> biological fluids,<sup>24</sup> vegetables, and plants.<sup>25-27</sup> The reduction of Fe<sup>III</sup>  
32  
33 underlying FRAP is a one-electron transfer reaction (*i.e.*,  $\text{Fe}^{\text{III}} + \text{e}^- \rightarrow \text{Fe}^{\text{II}}$ ), and no side  
34  
35 reactions have been recognized in a water solution. The principle of FRAP was applied  
36  
37 to analyze NPs' oxidative stress to serum media in the “ferric reducing ability of serum  
38  
39 (FRAS)<sup>19, 28</sup>” assay, yet no existing studies have applied this model reaction to directly  
40  
41 probe the reactivity of NP surface to our best knowledge.  
42  
43  
44  
45  
46

47 In this paper we report the use of ferric reducing assay to probe the surface reactivity  
48  
49 of two representative metallic NPs, gold (Au) and silver (Ag), and combine the assay  
50  
51 results with theoretical kinetic modeling to uncover electron transfer schemes at the NP-  
52  
53 solution interface. As a derivative assay from FRAP, our assay is named “ferric reducing  
54  
55  
56  
57  
58  
59  
60

1  
2  
3 ability of NPs (FRAN)". The FRAN assay allows recording  $\text{Fe}^{\text{II}}$  concentration at 0.2 s  
4 intervals, collecting adequate kinetic data as opposed to collecting only one reading by  
5 most traditional assays. We observed different kinetic patterns between Au and Ag NPs  
6 and developed two theoretical kinetic modeling frameworks to validate them. The two  
7 modeling frameworks correspond to two different interfacial electron transfer schemes  
8 uncovered by FRAN.  
9

## 10 11 12 13 14 15 16 17 18 19 20 21 22 23 24 25 26 27 28 29 30 31 32 33 34 35 36 37 38 39 40 41 42 43 44 45 46 47 48 49 50 51 52 53 54 55 56 57 58 59 60

**Chemicals.** Au (NanoXact, 0.05 mg/mL) and Ag (NanoXact, 0.02 mg/mL) nanospheres with nominal sizes of 20 nm were purchased from nanoComposix. TEM images (Figure S1) of these NPs show they are spherical with diameters narrowly distributed around 20 nm. Ferric Chloride ( $\text{FeCl}_3$ ) solution was prepared from iron(III) chloride hexahydrate ( $\text{FeCl}_3 \cdot 6\text{H}_2\text{O}$ ,  $\geq 98\%$ , Sigma-Aldrich, F2877). 2,4,6-Tris(2-pyridyl)-s-triazine (TPTZ) was purchased from Sigma Aldrich (93285). Acetate buffer (pH 3.6) was prepared from acetic acid (Fisher Brand, BP2401C-212) and sodium acetate trihydrate (ACS reagent,  $\geq 99\%$ , Sigma Aldrich, 236500). Safety data sheets for all used chemical materials are accessible from the manufactures with provided product numbers. Ultrapure water ( $18.2 \text{ M}\Omega \cdot \text{cm}$ , Barnstead GenPure xCAD Plus) was used to make solutions.

**FRAN assay.** Solutions for FRAN were prepared according to the FRAP assay.<sup>22</sup> A final FRAN assay solution was obtained by mixing 2.5 mL TPTZ solution (10 mM in a 40 mM HCl solution), 2.5 mL  $\text{FeCl}_3$  solution (20 mM in water), and 25 mL acetate buffer (0.3 M in water, pH=3.6) in a polystyrene centrifuge tube. For operation, 2.5 mL of the as-prepared FRAN solution was added into a 1-cm path length cuvette (Perfector Scientific, #9012), which was then placed in a portable UV-VIS absorbance spectrometer

(Ocean Optics, USB-ISS-UV/VIS and USB4000 light source). The interfacial reaction was initiated by adding an aliquot of NP stock solution into the cuvette to reach a desired concentration. The spectrometer was operated in an absorbance time-resolved reading mode at 593 nm (the primary absorbance peak of Fe<sup>II</sup>-TPTZ). The absorbance at 593 nm ( $A^{593}$ ) acquired was recorded every 0.2 s until a plateau was reached.  $A^{593}$  was converted to the concentration of Fe<sup>II</sup> ( $C_{\text{Fe}^{\text{II}}}$ ) using the known extinction coefficient of Fe<sup>II</sup>-TPTZ complex species ( $\epsilon=22600 \text{ L i mol}^{-1} \text{ i cm}^{-1}$ ) in the solution.

## RESULTS

Figure 1 shows the Fe<sup>II</sup> formation kinetics with Au and Ag NPs tested with FRAN. Fe<sup>II</sup> evolution for both NPs confirms that they are reactive and mediate electron transfer to Fe<sup>III</sup>. For both NPs, the kinetic change in  $C_{\text{Fe}^{\text{II}}}$  plateaued after ~100 s. The plateau values ( $C_{\text{Fe}^{\text{II}}}^{\text{p}}$ ) were determined by taking the mean of  $C_{\text{Fe}^{\text{II}}}$  from 150–200 s, in which period the increase of  $C_{\text{Fe}^{\text{II}}}$  is smaller than 0.05  $\mu\text{M}$ .  $C_{\text{Fe}^{\text{II}}}^{\text{p}}$  and was linearly dependent on the NP concentration for both Au and Ag NPs (Figure 2). Thus  $C_{\text{Fe}^{\text{II}}}^{\text{p}}$  was an indicator for net NP surface reactivity. This aligns well with the original FRAP assay using steady-state  $C_{\text{Fe}^{\text{II}}}$  to indicate the antioxidant power. Ag NPs had significantly higher reactivity than Au, regardless of whether the reactivity was normalized to mass (Figure 2a) or surface area (Figure 2b). The two NPs exhibited different shapes in the kinetic profile of  $C_{\text{Fe}^{\text{II}}}$  (Figure 1). Whereas Ag NPs exhibited a linear change in  $C_{\text{Fe}^{\text{II}}}$  until ~60 s before plateauing (Figure 1a), Au NPs exhibited a very fast increase in  $C_{\text{Fe}^{\text{II}}}$  within ~20 s followed by a non-linear gradual increase to a plateau after ~100 s. Additional

1  
2  
3 experiments were conducted across several NP concentrations and gave the same  
4  
5 observations. The distinct kinetic profiles indicate that the surface reaction scheme may  
6  
7 fundamentally differ between Ag and Au NPs.  
8  
9

## 11 12 13 **DISCUSSION**

14  
15 Observations summarized in Figure 1 and 2 bring about two questions: (1) does  $C_{\text{Fe}^{\text{II}}}^{\text{p}}$   
16  
17 adequately indicate NP surface reactivity in the applied FRAN assay?, and (2) what  
18  
19 electron transfer schemes can give rise to the different kinetic profile trends between Ag  
20  
21 and Au NPs? We hypothesized that the different kinetic profile trends between Ag and  
22  
23 Au contain critical information regarding NP surface reactivity, which is not reflected by  
24  
25 measurements under pseudo-equilibrium conditions (*i.e.*, upon reaching a reaction  
26  
27 plateau,  $C_{\text{Fe}^{\text{II}}}^{\text{p}}$  ).  
28  
29  
30

31  
32 If the reaction is governed by the first-order kinetics, an exponential function (*exp*)  
33  
34 should fit the Figure 1 data. Figure 3 shows that an exponential function provides an  
35  
36 excellent data fit for Ag but not for Au NPs. For Au, the *exp* underestimates the data at  
37  
38 the initial and the final period of time, and the data is fit better by a natural logarithm  
39  
40 function (*log*). Figures 3c and 3d provide residuals of fitting with *log* or *exp* functions for  
41  
42 the two NPs. Clearly, *exp* yields residuals much closer to zero than *log* for Ag, whereas  
43  
44 the opposite is true for Au. The same conclusion was achieved for data at all NP  
45  
46 concentrations.  
47  
48  
49

50  
51 To reveal the different surface reaction schemes between the Ag and Au NPs, we  
52  
53 developed theoretical models to explain the observed *exp* and *log* kinetic trends. The *exp*  
54  
55 trend given by the Ag NPs suggests the surface reaction is following first-order kinetics.  
56  
57  
58  
59  
60

1  
2  
3 As Fe<sup>III</sup> is dosed in excess compared to Ag NPs, the first-order kinetics suggests that Ag<sup>0</sup>  
4 atoms, which constitute Ag NPs, and Fe<sup>III</sup> ions randomly collide, react, and transform to  
5 Ag<sup>+</sup> and Fe<sup>II</sup>. As such, the assay reaction is a one-electron transfer redox process as  
6  
7



11  
12 This assumption is supported by the fact that oxidation favors Ag NPs' dissolution to  
13 form Ag<sup>+</sup>.<sup>29</sup> Skepticism upon the thermodynamic favorableness of reaction (1) may be  
14 raised by noting the recorded standard reducing potential ( $E^0$ ) of Ag<sup>+</sup>/Ag (0.799 V) is  
15 slightly higher than that of Fe<sup>3+</sup>/Fe<sup>2+</sup> (0.771 V).<sup>30</sup> But reaction (1) is able to proceed for  
16 two reasons: (1) it occurs in non-equilibrium and the high activity of Fe<sup>III</sup> creates a  
17 driving force compensating the assumed negative  $\Delta E^0 (= E_{\text{Fe}^{3+}/\text{Fe}^{2+}}^0 - E_{\text{Ag}^+/\text{Ag}^0}^0)$  according to  
18 the Nernst equation<sup>31</sup>, and (2)  $E^0$  of Ag<sup>+</sup>/Ag<sup>0</sup> for Ag<sup>0</sup> NPs is lower than that for bulk Ag<sup>32</sup>,  
19  
20  
21  
22  
23  
24  
25  
26  
27  
28  
29  
30  
31  
32  
33  
34  
35  
36  
37  
38  
39  
40  
41  
42  
43  
44  
45  
46  
47  
48  
49  
50  
51  
52  
53  
54  
55  
56  
57  
58  
59  
60

Reaction (1) is a heterogeneous reaction because Ag<sup>0</sup> and Fe<sup>III</sup> are in two different phases: the NP is solid, and the Fe<sup>III</sup> is in aqueous solution. The Ag<sup>0</sup> available for collision and reaction with Fe<sup>III</sup> can only be those on the NP surface, and they are not homogeneously distributed throughout the liquid phase like the Fe<sup>III</sup> ions. Consequently, a space in which the surface Ag<sup>0</sup> and Fe<sup>III</sup> are both homogeneously distributed should be constructed in the model to validate the first-order kinetics. We thus conceptualize a virtual layer with a thickness of  $\delta$  at the NP-water interface. The magnitude of  $\delta$  is taken

as small as what it requires to meet the approximation that surface  $\text{Ag}^0$  atoms and  $\text{Fe}^{\text{III}}$  ions are both homogeneously distributed within the layer and random collision between the two reactants occurs. As such, in the virtual space, reaction (1) approximates a homogeneous and pseudo first-order reaction, and  $\text{Ag}^0$  reaction rate can be written as

$$\frac{d(\nu_{\text{Ag}} \pi d^2 \delta)}{dt} = -k(\nu_{\text{Ag}} \pi d^2 \delta), \quad (2)$$

where  $\nu_{\text{Ag}} \pi d^2 \delta$  gives the total molarity of  $\text{Ag}^0$  within the assumed virtual layer, assuming the molar concentration of  $\text{Ag}^0$  is constant in this layer and equivalent to the molar density ( $\nu_{\text{Ag}}$ , in  $[\text{mol} \cdot \text{m}^{-3}]$ ) of the Ag NP. Meanings of all symbols hereafter are defined in a nomenclature table at the end. Each reacted  $\text{Ag}^0$  accounts for the formation of a  $\text{Fe}^{\text{II}}$ . A derivation (details are given in the ESI) from eq (2) leads to the  $\text{Fe}^{\text{II}}$  formation kinetics as

$$C_{\text{Fe}^{\text{II}}}(t) = C_{\text{Ag}^0,0} [1 - \exp(-k_{\text{obs}} t)] \quad (3)$$

As such, the *exp* kinetic trend in the Ag NP scenario is validated. From eq (2) to eq (3),  $d_0$  became an implicit part of  $C_{\text{Ag}^0,0}$ . Consequently, varying NP diameter can influence

$C_{\text{Ag}^0,0}$  through a defined relationship ( $C_{\text{Ag}^0,0} = \frac{1}{6} \pi d_0^3 \nu_{\text{Ag}} C_{\text{Ag NP}}^{\text{num}}$ ). As such, if the number of Ag nanoparticles is fixed in a working solution, the sensitivity towards initial NP diameter in the model simulations is analogous to varying  $C_{\text{Ag}^0,0}$ .

Au does not undergo redox-mediated dissolution as easily as Ag due to much higher standard reducing potential (at 298.15 K) of  $\text{Au}^+/\text{Au}$  (1.69 V) comparing to that of  $\text{Fe}^{3+}/\text{Fe}^{2+}$  (0.771 V).<sup>30</sup> Thus, a direct reaction between  $\text{Au}^0$  and  $\text{Fe}^{\text{III}}$  like in Reaction (1)

1  
2  
3 does not apply. However, the reaction occurring in the Au scenario suggests Au NPs  
4  
5 indeed mediate electron transfer to reduce Fe<sup>III</sup>. We related the reaction to the property of  
6  
7 Au being a good conductor and assumed an “electron discharge” mechanism guides the  
8  
9 surface reaction. When a NP contacts water, surface charge develops due to the chemical  
10  
11 potential difference between the solid and water phases. This “charging process” can be  
12  
13 imposed by the polar water molecules in an extremely short time-scale<sup>35</sup> and leads to a  
14  
15 surface potential, which can be related to the measurable “zeta-potential” between  
16  
17 particle surface and the bulk water. We analogize the NP to be a very small electrode,  
18  
19 which carries an initial surface charge density ( $q_0$ ) and potential ( $\Psi_0$ ). Fe<sup>III</sup> is reduced at  
20  
21 the NP or the “electrode” surface by taking the stored “free” electrons ( $e^-$ ) from the solid  
22  
23 phase. The Au NP itself is not consumed, *i.e.*, no Au<sup>+</sup> dissolves from Au<sup>0</sup>. The Fe<sup>III</sup>  
24  
25 reduction is described by a half reaction:  
26  
27  
28  
29



31  
32 The Butler-Volmer equation guides the kinetics of reaction (4) on an electrode as:  
33  
34

$$35 \quad i = F A k_0 C_{\text{Fe}^{\text{III}}} \exp\left(-\frac{\alpha F \eta}{RT}\right). \quad (5)$$

36  
37 The overpotential of the electrode,  $\eta$ , is controlled by the charge carried on the Au  
38  
39 surface, which constructs a capacitor with the bulk solution at the interface. Eq (5) can  
40  
41 be further treated by a capacitor model<sup>36, 37</sup> by substituting  $Q/C$  for  $\eta$  and by writing  $i$  as  
42  
43 the time derivative of  $Q$ :  
44  
45  
46  
47  
48

$$49 \quad \frac{dQ}{dt} = F A k_0 C_{\text{Fe}^{\text{III}}} \exp\left(-\frac{\alpha F Q}{R T C}\right). \quad (6)$$

Eq (7) is a differential equation with respect to  $Q(t)$ . Solving eq (7) and associated derivations (details in the ESI) and additional derivations give rise to the  $\text{Fe}^{\text{II}}$  formation kinetic equation:

$$C_{\text{Fe}^{\text{II}}}(t) = LC_{\text{Au NP}}^{\text{mass}} A_{\text{m, Au NP}} C_S \log(1 + KC_{\text{Fe}^{\text{III}}}t); \quad (7a)$$

$$L = \frac{RT}{\alpha F^2}; \quad (7b)$$

$$K = \frac{k_0}{LC_S} \exp\left(-\frac{q_0}{LFC_S}\right). \quad (7c)$$

As such, the *log* kinetic trend in the Au NP scenario is justified.

The two theoretical models assumed no change in surface area change due to particle agglomeration or aggregation, which were avoided by the electrostatic stability of the nanoparticles and by the effective mechanical mixing in the experiment. Dashed lines in Figure 1 show data fits by eq (3) for Ag and eq (7) for Au at multiple NP concentrations.  $C_{\text{Ag}^0,0}$  and  $k_{\text{obs}}$  in eq (3), and  $C_S$  and  $K$  in eq (8) were treated as unknown parameters and were determined by data regression. Fitted parameter values were plotted over the concentration of NPs in Figure 4. Figure 4a shows the independence of  $k_{\text{obs}}$  on Ag concentration, which was expected because it is only a derived parameter from  $k$  in eq (2). The fitted  $C_{\text{Ag}^0,0}$  was converted to  $\text{Ag}^0$  mass concentration ( $C_{\text{Ag}^0,0}^{\text{mass}}$ ), which is plotted as the right axis in Figure 4a. This parameter resulted in a 1:1 line with the experimentally dosed mass concentration of Ag NPs, proving the model's validity. The final molar concentration of  $\text{Fe}^{\text{II}}$  (*i.e.*,  $C_{\text{Fe}^{\text{II}}}^{\text{p}}$ ) was also equivalent to the total molar concentration of Ag (Figure S2). This implies that all Ag atoms constituting the NPs, including those in the particle core, have been exposed to and reacted with  $\text{Fe}^{\text{III}}$  via dissolution. We also

1  
2  
3 observed that the surface plasmon absorbance of Ag NPs dissipated along with the  
4  
5 formation of Fe<sup>II</sup> and reached zero at the end reaction (Figure S3). These findings  
6  
7 support the one-electron transfer of reaction (1) and the assumption that all the Ag NPs  
8  
9 were oxidized to Ag<sup>+</sup> at the end of the reaction. The fitted  $C_S$  is independent of Au NP  
10  
11 concentrations (Figure 4b), suggesting  $C_S$  is an intensive property of the NP. This is  
12  
13 consistent with the classical Poisson-Boltzmann theory derived models that predict the  
14  
15 surface specific capacity of colloids in a solution depends only on the colloids material  
16  
17 and solution constitution<sup>38</sup>. The fitted  $K$  value increased with Au NP dosage (Figure 4b).  
18  
19 However, eq (7c) suggests that  $K$  is a function of  $k_0$ ,  $q_0$ , and  $C_S$  ( $\alpha$  is assumed to be  
20  
21  $0.5^{37}$ ). We did not expect these three parameters would vary with Au NP concentration.  
22  
23 The observed variance of  $K$  may be caused by mass transfer limitations, which would  
24  
25 lead to the observed  $k_0$  increases with the NP concentration.  
26  
27  
28  
29  
30  
31  
32

## 33 CONCLUSIONS

34  
35 We substantiated two points in this work. First, we successfully applied the ferric  
36  
37 reducing assay to assess the surface reactivity of metallic NPs with respect to donating  
38  
39 electrons. The demonstrated FRAN is based on a simple one-electron redox reaction,  
40  
41 ruling out interfering side reactions carried by many other similar-type assays. Second,  
42  
43 through theoretically modeling the assay reaction kinetics, we revealed two different  
44  
45 electron transfer schemes. Represented by the Ag NP, Fe<sup>III</sup> is reduced directly by NP  
46  
47 surface atoms, with the material transforming to other species (*e.g.*, Ag<sup>0</sup> transforms to  
48  
49 Ag<sup>+</sup>). The electron transfer occurs in a “space” that is in close proximity to the NP  
50  
51 surface and bounds the homogeneous and random collision of reactants. Alternatively,  
52  
53  
54  
55  
56  
57  
58  
59  
60

represented by the Au NP, the reduction of Fe<sup>III</sup> can occur similar to the principles of an electrode reaction as the NP acts as a microelectrode and the NP-water interface acts as a capacitor that is discharged as Fe<sup>III</sup> accepts electrons from the NP. The distinct electron transfer schemes corroborate that the apparent redox reactions mediated by different metallic NPs or colloids can be governed by different reaction mechanisms, which have been often overlooked when only reactant or product in one reaction state being detected. This can be true not only to many reactions enabling NP reactivity assays, but also to those in which the NP is technologized (*e.g.*, as a catalyst). There are numerous direct routes of nano-Ag release to the environment<sup>39</sup>, but fewer exist for nano-Au. Therefore, in this paper Ag and Au represent surrogates of NPs with different properties (redox-drive dissolution Ag-NP *vs.* low solubility Au-NP). Knowing the electron transfer scheme mediated by NPs can lead to improved understanding of the surface reactivity nature in reactivity assays, and more efficient technology development for environmental applications of NPs. Our theoretical models and insights can inform other heterogeneous electron transfer processes in environmental systems, such as the transformation of iron oxides in the aqueous environment<sup>40, 41</sup> and mineral-catalyzed contaminant degradation.<sup>42</sup> Overall, this work provides an approach that is easy to perform experimentally and is linked to sophisticated modeling pointing to the electron transfer schemes.

#### NOMENCLATURE

Symbol	Meaning and unit in SI	Related equation
$A$	Total surface area of NPs in a solution, [m <sup>2</sup> ].	(5), (6), (s8), and (s9)
$A_{m,AuNP}$	Specific surface area of Au NPs, [m <sup>2</sup> · kg <sup>-1</sup> ].	(8)
$C$	Total capacitance of NPs in a solution, [F].	(6), (s8), and (s9)

1			
2			
3			
4	$C_S$	Surface specific capacitance of NPs in a solution, [ $F \cdot m^{-2}$ ].	(7)
5			
6			
7	$C_{Ag^0,0}$	Initial molar concentration of $Ag^0$ in the solution, [ $mol \cdot m^{-3}$ ].	(3) and (s7)
8			
9			
10			
11	$C_{AgNP}^{num}$	Number concentration of Ag NPs in a solution, [ $m^{-3}$ ].	(s5) and (s6)
12			
13			
14	$C_{AuNP}^{mass}$	Mass concentration of Au NPs in a solution, [ $kg \cdot m^{-3}$ ].	(7)
15			
16			
17			
18	$C_{Fe^{III}}$	Molar concentration of $Fe^{III}$ in a solution, [ $mol \cdot m^{-3}$ ].	(5)-(7), (s8), and (s9)
19			
20			
21			
22	$C_{Fe^{II}}$	Molar concentration of $Fe^{II}$ in a solution, [ $mol \cdot m^{-3}$ ].	(3), (7), (s5)-(s7), and (s9)
23			
24			
25	$n_{Fe^{II}}$	Molarity of $Fe^{II}$	(s4)
26			
27			
28	$d$	Diameter of a NP, [m].	(s1)-(s5)
29			
30	$d_0$	Initial diameter of a NP, [m].	(s3)-(s5)
31			
32			
33	$F$	Faraday constant, 96485 [ $C \cdot mol^{-3}$ ].	(5)-(7), (s8), and (s9)
34			
35	$i$	Current, [A].	(5)
36			
37	$k$	Pseudo first-order rate constant, [ $s^{-1}$ ].	(2), (s1)-(s3), and (s6)
38			
39			
40	$k_0$	Standard rate constant for an electrode reaction, [ $m \cdot s^{-1}$ ].	(5)-(7), (s8), and (s9)
41			
42			
43	$k_{obs}$	Observed rate constant, [ $s^{-1}$ ].	(3) and (s7)
44			
45			
46	$Q$	Total charge on NPs' surface, [C].	(6), (7), (s8), and (s9)
47			
48	$Q_0$	Initial total charge on NPs' surface, [C].	(s8) and (s9)
49			
50			
51	$q_0$	Initial surface charge density of NPs in a solution, [ $C \cdot m^{-2}$ ].	(7)
52			
53			
54	$R$	Ideal gas constant, 8.314 [ $J \cdot mol^{-1}$ ].	(5)-(7), (s8) and (s9)
55			
56			
57			
58			
59			
60			

$t$	Time, [s].	(2), (3), (6), (7), (s1)-(s3), and (s5)-(s9)
$T$	Temperature, [K].	(5)-(7), and (s8)-(s9)
$\alpha$	Transfer coefficient, dimensionless.	(5)-(7), and (s8)-(s9)
$\eta$	Over potential, [V].	(5)
$\nu_{\text{Ag}}$	Molar density of a Ag NP, [ $\text{mol} \cdot \text{m}^{-3}$ ].	(2), (s1) and (s4)-(s6)
$\delta$	Thickness of the virtual interfacial layer, [m].	(2) and (s1)

---

### ACKNOWLEDGEMENTS

Partial funding was provided from the National Science Foundation (CBET1507750) via Grant Opportunities for Academic Liaison with Industry (GOALI) jointly with the semiconductor research corporation (SRC, Task 425.052), US Environmental Protection Agency through the STAR program (RD83558001), and by the NSF Nanosystems Engineering Research Center for Nanotechnology-Enabled Water Treatment (EEC-1449500).

### REFERENCES

- Hvolbaek, B.; Janssens, T. V. W.; Clausen, B. S.; Falsig, H.; Christensen, C. H.; Norskov, J. K., Catalytic activity of Au nanoparticles. *Nano Today* **2007**, 2, (4), 14-18.
- Zhang, L.; Gu, F. X.; Chan, J. M.; Wang, A. Z.; Langer, R. S.; Farokhzad, O. C., Nanoparticles in medicine: Therapeutic applications and developments. *Clin Pharmacol Ther* **2008**, 83, (5), 761-769.
- Shahverdi, A. R.; Fakhimi, A.; Shahverdi, H. R.; Minaian, S., Synthesis and effect of silver nanoparticles on the antibacterial activity of different antibiotics against

- 1  
2  
3 Staphylococcus aureus and Escherichia coli. *Nanomedicine: Nanotechnology, Biology*  
4 *and Medicine* **2007**, 3, (2), 168-171.
- 5  
6  
7  
8 4. Lok, C.-N.; Ho, C.-M.; Chen, R.; He, Q.-Y.; Yu, W.-Y.; Sun, H.; Tam, P. K.-H.;  
9  
10 Chiu, J.-F.; Che, C.-M., Silver nanoparticles: partial oxidation and antibacterial activities.  
11  
12 *JBIC Journal of Biological Inorganic Chemistry* **2007**, 12, (4), 527-534.
- 13  
14  
15 5. Perelshtein, I.; Applerot, G.; Perkas, N.; Guibert, G.; Mikhailov, S.; Gedanken,  
16  
17 A., Sonochemical coating of silver nanoparticles on textile fabrics (nylon, polyester and  
18  
19 cotton) and their antibacterial activity. *Nanotechnology* **2008**, 19, (24).
- 20  
21  
22 6. Asati, A.; Santra, S.; Kaittanis, C.; Nath, S.; Perez, J. M., Oxidase-Like Activity  
23  
24 of Polymer-Coated Cerium Oxide Nanoparticles. *Angew Chem Int Edit* **2009**, 48, (13),  
25  
26 2308-2312.
- 27  
28  
29 7. Sakaue, Y.; Kim, J.; Miyamoto, Y., Effects of TAT-conjugated platinum  
30  
31 nanoparticles on lifespan of mitochondrial electron transport complex I-deficient  
32  
33 *Caenorhabditis elegans*, nuo-1. *International journal of nanomedicine* **2010**, 5, 687.
- 34  
35  
36 8. Thill, A.; Zeyons, O.; Spalla, O.; Chauvat, F.; Rose, J.; Auffan, M.; Flank, A. M.,  
37  
38 Cytotoxicity of CeO<sub>2</sub> nanoparticles for Escherichia coli. Physico-chemical insight of the  
39  
40 cytotoxicity mechanism. *Environ. Sci. Technol.* **2006**, 40, (19), 6151-6156.
- 41  
42  
43 9. Karlsson, H. L.; Cronholm, P.; Hedberg, Y.; Tornberg, M.; De Battice, L.;  
44  
45 Svedhem, S.; Wallirider, I. O., Cell membrane damage and protein interaction induced by  
46  
47 copper containing nanoparticles-Importance of the metal release process. *Toxicology*  
48  
49 **2013**, 313, (1), 59-69.
- 50  
51  
52 10. Xia, T.; Kovoichich, M.; Brant, J.; Hotze, M.; Sempf, J.; Oberley, T.; Sioutas, C.;  
53  
54 Yeh, J. I.; Wiesner, M. R.; Nel, A. E., Comparison of the abilities of ambient and  
55  
56  
57  
58  
59  
60

1  
2  
3 manufactured nanoparticles to induce cellular toxicity according to an oxidative stress  
4 paradigm. *Nano Letters* **2006**, *6*, (8), 1794-1807.

7  
8 11. Kroll, A.; Dierker, C.; Rommel, C.; Hahn, D.; Wohlleben, W.; Schulze-Isfort, C.;  
9  
10 Gobbert, C.; Voetz, M.; Hardinghaus, F.; Schnekenburger, J., Cytotoxicity screening of  
11  
12 23 engineered nanomaterials using a test matrix of ten cell lines and three different  
13  
14 assays. *Particle and Fibre Toxicology* **2011**, *8*.

15  
16  
17 12. Lee, S.; Bi, X. Y.; Reed, R. B.; Ranville, J. F.; Herckes, P.; Westerhoff, P.,  
18  
19 Nanoparticle Size Detection Limits by Single Particle ICP-MS for 40 Elements. *Environ.*  
20  
21 *Sci. Technol.* **2014**, *48*, (17), 10291-10300.

22  
23  
24 13. Venkatesan, A. K.; Reed, R. B.; Lee, S.; Bi, X.; Hanigan, D.; Yang, Y.; Ranville,  
25  
26 J. F.; Herckes, P.; Westerhoff, P., Detection and Sizing of Ti-Containing Particles in  
27  
28 Recreational Waters Using Single Particle ICP-MS. *Bulletin of environmental*  
29  
30 *contamination and toxicology* **2018**, *100*, (1), 120-126.

31  
32  
33 14. Venkatesan, A.; Rodriguez, B.; Marcotte, A.; Bi, X.; Schoepf, J.; Ranville, J. F.;  
34  
35 Herckes, P.; Westerhoff, P., Using single particle ICP-MS for monitoring metal-  
36  
37 containing particles in tap waters. *Environmental Science: Water Research & Technology*  
38  
39 **2018**.

40  
41  
42 15. Wunder, S.; Lu, Y.; Albrecht, M.; Ballauff, M., Catalytic Activity of Faceted  
43  
44 Gold Nanoparticles Studied by a Model Reaction: Evidence for Substrate-Induced  
45  
46 Surface Restructuring. *Acs Catal* **2011**, *1*, (8), 908-916.

47  
48  
49 16. Carregal-Romero, S.; Perez-Juste, J.; Herves, P.; Liz-Marzan, L. M.; Mulvaney,  
50  
51 P., Colloidal Gold-Catalyzed Reduction of Ferrocyanate (III) by Borohydride Ions: A  
52  
53 Model System for Redox Catalysis. *Langmuir* **2010**, *26*, (2), 1271-1277.  
54  
55  
56  
57  
58  
59  
60

- 1  
2  
3 17. Corredor, C.; Borysiak, M. D.; Wolfer, J.; Westerhoff, P.; Posner, J. D.,  
4  
5 Colorimetric Detection of Catalytic Reactivity of Nanoparticles in Complex Matrices.  
6  
7 *Environ. Sci. Technol.* **2015**, *49*, (6), 3611-3618.  
8  
9  
10 18. Bartosz, G., Use of spectroscopic probes for detection of reactive oxygen species.  
11  
12 *Clinica Chimica Acta* **2006**, *368*, (1), 53-76.  
13  
14  
15 19. Pal, A. K.; Hsieh, S. F.; Khatri, M.; Isaacs, J. A.; Demokritou, P.; Gaines, P.;  
16  
17 Schmidt, D. F.; Rogers, E. J.; Bello, D., Screening for oxidative damage by engineered  
18  
19 nanomaterials: a comparative evaluation of FRAS and DCFH. *Journal of Nanoparticle*  
20  
21 *Research* **2014**, *16*, (1).  
22  
23  
24 20. Lu, S.; Duffin, R.; Poland, C.; Daly, P.; Murphy, F.; Drost, E.; MacNee, W.;  
25  
26 Stone, V.; Donaldson, K., Efficacy of simple short-term in vitro assays for predicting the  
27  
28 potential of metal oxide nanoparticles to cause pulmonary inflammation. *Environmental*  
29  
30 *health perspectives* **2009**, *117*, (2), 241.  
31  
32  
33 21. Li, Y.; Zhang, W.; Niu, J.; Chen, Y., Mechanism of photogenerated reactive  
34  
35 oxygen species and correlation with the antibacterial properties of engineered metal-  
36  
37 oxide nanoparticles. *Acs Nano* **2012**, *6*, (6), 5164-5173.  
38  
39  
40 22. Benzie, I. F.; Strain, J., The ferric reducing ability of plasma (FRAP) as a measure  
41  
42 of “antioxidant power”: the FRAP assay. *Analytical biochemistry* **1996**, *239*, (1), 70-76.  
43  
44  
45 23. Pulido, R.; Bravo, L.; Saura-Calixto, F., Antioxidant activity of dietary  
46  
47 polyphenols as determined by a modified ferric reducing/antioxidant power assay.  
48  
49 *Journal of Agricultural and Food Chemistry* **2000**, *48*, (8), 3396-3402.  
50  
51  
52 24. Benzie, I. F. F.; Strain, J. J., Ferric reducing antioxidant power assay: Direct  
53  
54 measure of total antioxidant activity of biological fluids and modified version for  
55  
56  
57  
58  
59  
60

simultaneous measurement of total antioxidant power and ascorbic acid concentration.

*Method Enzymol* **1999**, *299*, 15-27.

25. Ou, B. X.; Huang, D. J.; Hampsch-Woodill, M.; Flanagan, J. A.; Deemer, E. K., Analysis of antioxidant activities of common vegetables employing oxygen radical absorbance capacity (ORAC) and ferric reducing antioxidant power (FRAP) assays: A comparative study. *Journal of Agricultural and Food Chemistry* **2002**, *50*, (11), 3122-3128.

26. Hajimahmoodi, M.; Hanifeh, M.; Oveisi, M. R.; Sadeghi, N.; Jannat, B., Determination of total antioxidant capacity of green teas by the ferric reducing/antioxidant power assay. *Iran J Environ Healt* **2008**, *5*, (3), 167-172.

27. Benzie, I. F. F.; Szeto, Y. T., Total antioxidant capacity of teas by the ferric reducing/antioxidant power assay. *Journal of Agricultural and Food Chemistry* **1999**, *47*, (2), 633-636.

28. Hellack, B.; Nickel, C.; Albrecht, C.; Kuhlbusch, T. A. J.; Boland, S.; Baeza-Squiban, A.; Wohlleben, W.; Schins, R. P. F., Analytical methods to assess the oxidative potential of nanoparticles: a review. *Environ Sci-Nano* **2017**, *4*, (10), 1920-1934.

29. Liu, J. Y.; Hurt, R. H., Ion Release Kinetics and Particle Persistence in Aqueous Nano-Silver Colloids. *Environ. Sci. Technol.* **2010**, *44*, (6), 2169-2175.

30. Bratsch, S. G., Standard electrode potentials and temperature coefficients in water at 298.15 K. *Journal of Physical and Chemical Reference Data* **1989**, *18*, (1), 1-21.

31. The Nernstian description of the electromotive force (*emf*) for reaction (1) is

$$emf = \Delta E^0 + \frac{RT}{F} \ln \left( \frac{a_{\text{Fe}^{\text{III}}} a_{\text{Ag}^0}}{a_{\text{Fe}^{\text{II}}} a_{\text{Ag}^+}} \right), \text{ where } \Delta E^0 = E_{\text{Fe}^{3+}/\text{Fe}^{2+}}^0 - E_{\text{Ag}^+/\text{Ag}^0}^0. \text{ Even if } \Delta E^0 \text{ is}$$

negative predicted by typical  $E^0$  data, e.g.,  $\Delta E^0 = (0.771 - 0.799) \text{ V} = -0.028 \text{ V}$ , the second term on the right side can compensate it and make the overall emf positive. For instance, assuming  $C_{\text{Ag}^0,0}^{\text{mass}} = 400 \mu\text{g/L}$ ,  $a_{\text{Ag}^0} = 1$ , and activity is approximated by concentration,

$\frac{RT}{F} \ln \left( \frac{a_{\text{Fe}^{\text{III}}} a_{\text{Ag}^0}}{a_{\text{Fe}^{\text{II}}} a_{\text{Ag}^+}} \right)$  is estimated to be 0.3 V when all Ag is dissolved at the end of the

reaction, acting as a dominant component to the overall *emf*.

32. Henglein, A., Physicochemical properties of small metal particles in solution: "microelectrode" reactions, chemisorption, composite metal particles, and the atom-to-metal transition. *The Journal of Physical Chemistry* **1993**, *97*, (21), 5457-5471.

33. Ivanova, O. S.; Zamborini, F. P., Size-dependent electrochemical oxidation of silver nanoparticles. *Journal of the American Chemical Society* **2009**, *132*, (1), 70-72.

34. Plieth, W., Electrochemical properties of small clusters of metal atoms and their role in the surface enhanced Raman scattering. *The Journal of Physical Chemistry* **1982**, *86*, (16), 3166-3170.

35. Hunter, R. J.; Ottewill, R. H., *Zeta potential in colloid science : principles and applications*. Academic Press: London ; New York, 1981; p xi, 386 p.

36. Henglein, A.; Lilie, J., Storage of Electrons in Aqueous-Solution - the Rates of Chemical Charging and Discharging the Colloidal Silver Microelectrode. *Journal of the American Chemical Society* **1981**, *103*, (5), 1059-1066.

37. Bard, A. J.; Faulkner, L. R., *Electrochemical methods : fundamentals and applications*. 2nd ed.; John Wiley: New York ; Chichester England, 2001; p xxi, 833 p.

38. Ohshima, H., *Theory of colloid and interfacial electric phenomena*. Elsevier Academic Press: Amsterdam ; New York, 2006; p xvi, 473 p.

- 1  
2  
3 39. Hochella, M. F.; Mogk, D. W.; Ranville, J.; Allen, I. C.; Luther, G. W.; Marr, L.  
4 C.; McGrail, B. P.; Murayama, M.; Qafoku, N. P.; Rosso, K. M., Natural, incidental, and  
5 engineered nanomaterials and their impacts on the Earth system. *Science* **2019**, *363*,  
6 (6434), eaau8299.  
7  
8  
9  
10  
11  
12 40. Friedrich, A. J.; Helgeson, M.; Liu, C.; Wang, C.; Rosso, K. M.; Scherer, M. M.,  
13 Iron atom exchange between hematite and aqueous Fe (II). *Environ. Sci. Technol.* **2015**,  
14 *49*, (14), 8479-8486.  
15  
16  
17  
18  
19 41. Cwiertny, D. M.; Hunter, G. J.; Pettibone, J. M.; Scherer, M. M.; Grassian, V. H.,  
20 Surface chemistry and dissolution of  $\alpha$ -FeOOH nanorods and microrods: Environmental  
21 implications of size-dependent interactions with oxalate. *The Journal of Physical*  
22 *Chemistry C* **2008**, *113*, (6), 2175-2186.  
23  
24  
25  
26  
27  
28 42. Li, F.; Li, X.; Li, X.; Liu, T.; Dong, J., Heterogeneous photodegradation of  
29 bisphenol A with iron oxides and oxalate in aqueous solution. *Journal of colloid and*  
30 *interface science* **2007**, *311*, (2), 481-490.  
31  
32  
33  
34  
35  
36  
37  
38  
39  
40  
41  
42  
43  
44  
45  
46  
47  
48  
49  
50  
51  
52  
53  
54  
55  
56  
57  
58  
59  
60

1  
2  
3 **Ferric reducing reactivity assay with theoretical kinetic modeling uncovers electron**  
4  
5 **transfer schemes of metallic-nanoparticle-mediated redox in water solutions**  
6

7  
8 Xiangyu Bi\* and Paul Westerhoff  
9

10  
11  
12 School of Sustainable Engineering and the Built Environment, Arizona State University,  
13  
14 Tempe, Arizona, USA  
15

16  
17 \*Correspondence: E: xiangyu.bi@asu.edu  
18

19 In preparation for submission to *Environmental Science: Nano*  
20  
21  
22  
23  
24  
25  
26  
27  
28  
29  
30  
31  
32  
33  
34  
35  
36  
37  
38  
39  
40  
41  
42  
43  
44  
45  
46  
47  
48  
49  
50  
51  
52  
53  
54  
55  
56  
57  
58  
59  
60

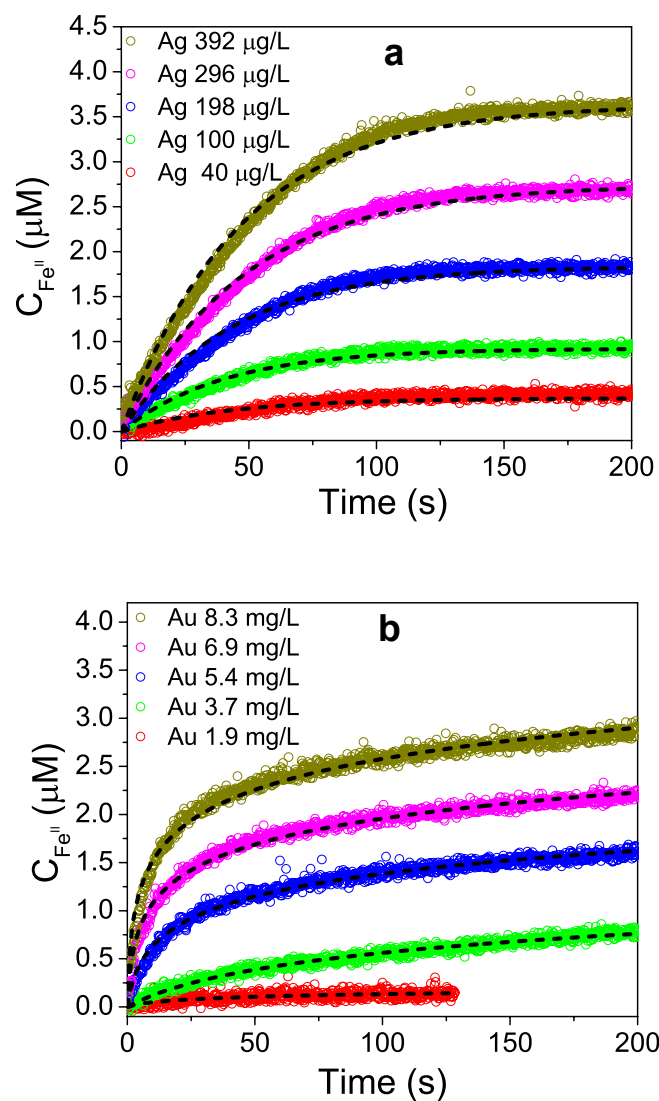


**Figure 1.** Kinetics profiles for Ag (a) and Au (b) NPs tested by FRAN at different concentrations. Markers are experimental data, and dashed lines are model simulation results.

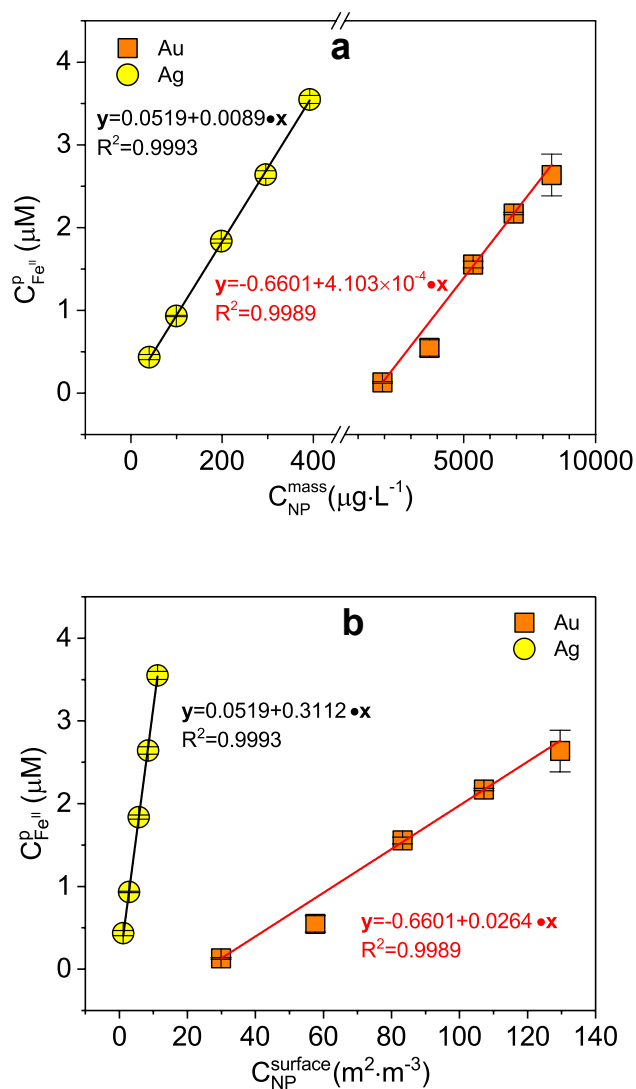


**Figure 2.** The plateaued Fe<sup>II</sup> concentration ( $C_{\text{Fe}^{\text{II}}}^{\text{p}}$ ) as a function of NP mass

concentration ( $C_{\text{NP}}^{\text{mass}}$ ) (a) and of NP surface concentration ( $C_{\text{NP}}^{\text{surface}}$ ) (b) for Au and Ag

NPs.  $C_{\text{NP}}^{\text{surface}}$  was converted from  $C_{\text{NP}}^{\text{mass}}$  based on spherical geometry of Ag and Au NPs,

i.e.,  $C_{\text{NP}}^{\text{surface}} = 6i C_{\text{NP}}^{\text{mass}} / (\rho d)$ , where  $\rho$  and  $d$  are the density and diameter of NPs,

respectively.

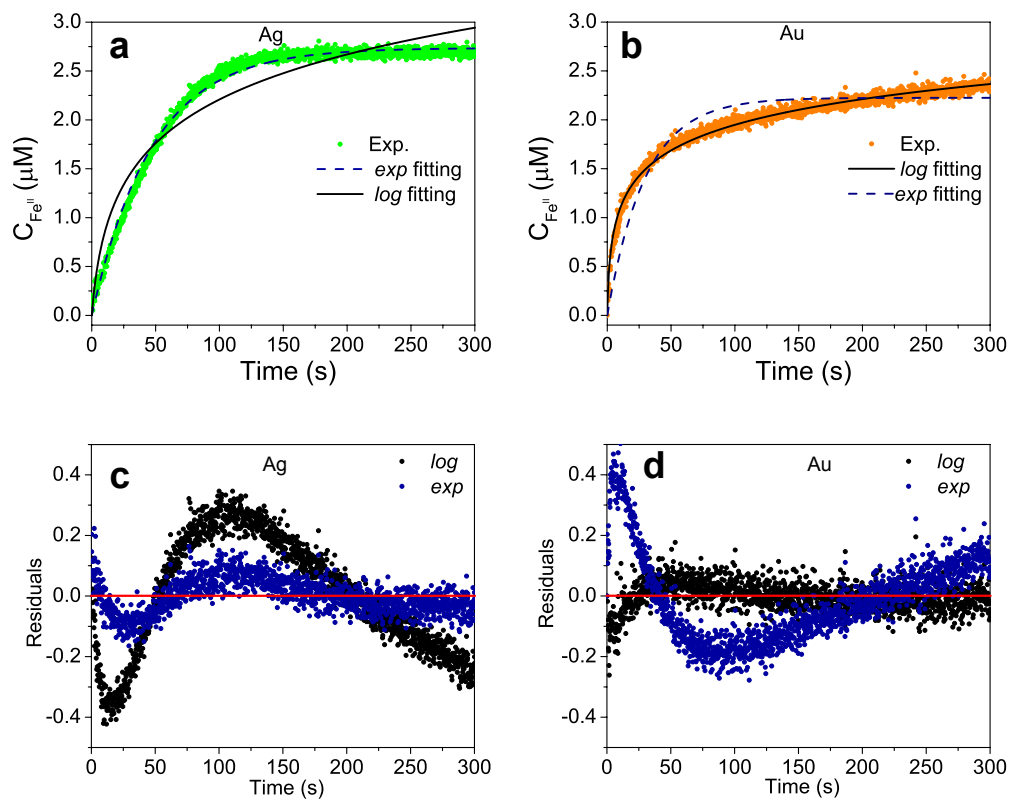


**Figure 3.** Comparison of the *exp* and *log* fitting for Ag NPs at 296  $\mu g/L$  (a) and Au NPs at 6.9 mg/L (b), and the residuals of fitting ((c) and (d)) for all cases.

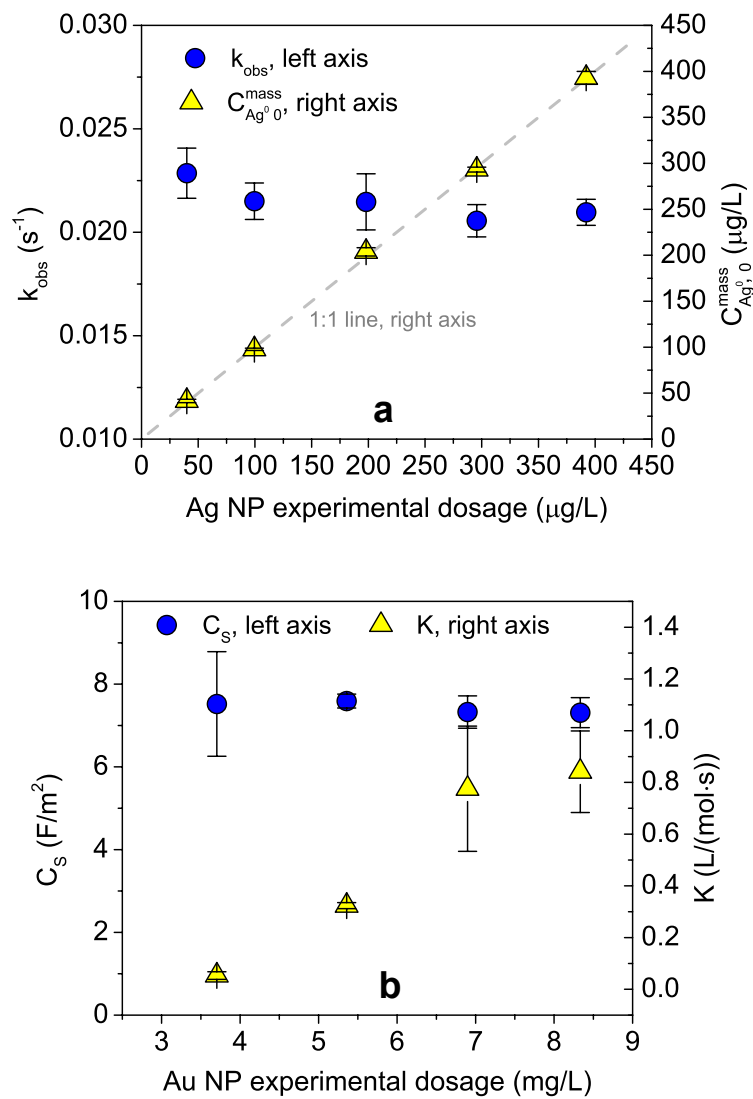


**Figure 4.** Fitted parameter values versus NP experimental dosage (as mass concentration) for Ag (a) and Au (b).

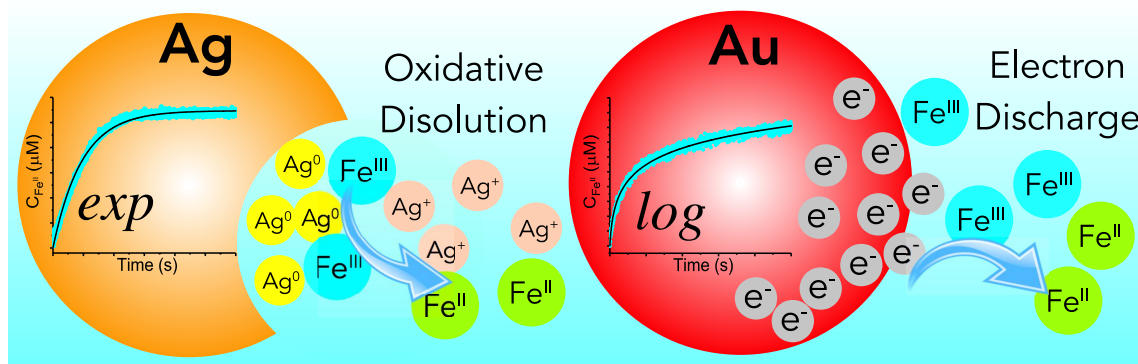
1  
2  
3 **Ferric reducing reactivity assay with theoretical kinetic modeling uncovers electron**  
4 **transfer schemes of metallic-nanoparticle-mediated redox in water solutions**  
5  
6

7 Xiangyu Bi\* and Paul Westerhoff

8  
9  
10  
11  
12 School of Sustainable Engineering and the Built Environment, Arizona State University, Tempe,  
13  
14 Arizona, USA

15  
16  
17 \*Correspondence: E: xiangyu.bi@asu.edu

18  
19 In preparation for submission to *Environmental Science: Nano*  
20  
21  
22  
23  
24  
25  
26  
27  
28



41 TOC art

42  
43  
44  
45  
46  
47  
48  
49  
50  
51  
52  
53  
54  
55  
56  
57  
58  
59  
60